CrossMark

Stability of LCL-filtered grid-connected inverters with capacitor current feedback active damping considering controller time delays

Wei XIA[1] , Jinsong KANG[1]

MPCE

Abstract This paper investigates the stability of LCL-filtered grid-connected inverters with capacitor current feedback (CCF) active damping. The impact of time delays in the digital controller on active damping and its equivalent virtual impedance is analyzed. The inherent relationship between these time delays and stability is illustrated. Specially, a critical value of the CCF active damping coefficient $k_{\mathrm{damp\_c}}$ is proposed to define three distinct regions of stability evaluation. If $k_{\mathrm{damp\_c}} > 0$, a sufficient but smaller damping coefficient ($k_{\mathrm{damp}} < k_{\mathrm{damp\_c}}$) is recommended as optimum damping solution; if $k_{\mathrm{damp\_c}} = 0$, system will be unstable irrespective of active damping; and if $k_{\mathrm{damp\_c}} < 0$, active damping is not necessary to design a stable system. Necessary conditions to ensure stability are identified; guidelines for controller design are then presented to optimize the performance of active damping and dynamic response. Simulation and experimental results confirm the presented analysis.

Keywords LCL filter, Grid-connected inverter, Controller time delays, Stability

1 Introduction

With the increasing penetration of distributed energy generation in power grids, grid-connected inverters become an indispensable component of modern power systems [1, 2]. A filter is necessary in a converter system to improve the performance of harmonic attenuation. Among filter designs, the LCL filter is attracting more attention because of its much lower weight and size, compared to single L filter. However, the LCL filter introduces substantial complexities into controller design due to the resonance phenomenon. Thus, damping solutions are needed to stabilize the converter system.

Passive damping by inserting a resistor into the filter is a direct and reliable solution. It has been proved that a resistor connected in parallel with the filter capacitor has an optimal magnitude characteristic for damping both in low and high frequency ranges, but collateral effects of high power losses are unaffordable [3]. To overcome this drawback, various active damping strategies are proposed to substitute the physical resistor by adding a feedback in the controller, which can be proportional to the capacitor current [4–6], or to the first-order differential of capacitor voltage [7], or to the second-order differential of the grid-side current [8, 9]. All of these damping strategies can be applied as a virtual resistor with the equivalently optimal performance, but proportional computation is more accurate compared with differential approximation in digital controller. Reference [10] found that an inverter-side current feedback (ICF) control loop is naturally stable, and this is equivalent to adding an inherent capacitor current feedback (CCF) term to the forward path of the direct control loop of the grid current; in other words, active damping is achieved by CCF. Therefore, in this paper, CCF active damping is adopted for its

STATE GRID
STATE GRID ELECTRIC POWER RESEARCH INSTITUTE

accuracy and simplicity when grid current is to be controlled directly.

Despite a vast amount of literature that has been published on the subject of LCL filter in grid-connected inverters, there is still no consensus on a stability evaluation method accounting for computation and pulse width modulation (PWM) delays [11–17]. Reference [11] presented pioneering research on active damping in discrete-time domain taking time delays into account, and concluded that discrete-time active damping is not always stable, depending on the ratio of resonance frequency to sampling frequency. Then [12] identified three distinct regions of LCL filter resonance frequency separated by one sixth of the sampling frequency ($f_s/6$), named the critical resonance frequency. They also proposed a design method for a digital controller in the two stable regions. Similar conclusions were also drawn in [13, 14]. However, these papers do not provide sufficient explanation of the inherent relationship between active damping and controller time delays. Reference [15] demonstrated the effect of delays on active damping performance, where the virtual impedance model consisting of a resistance paralleled with a reactance was proposed, but the conclusion is incomplete since active damping is not required when the LCL filter is operated in the high resonance frequency region. Reference [16] indicated that a single loop of grid-side current feedback without any additional active damping can be naturally stabilized by the inherent damping characteristics owing to time delays in the digital control system. Besides, [17] analyzed the relationship between time delays and stability of single loop controlled inverters, and used an intentional time delay addition method as inherent damping to improve stability of the grid-side current feedback loop.

In summary, the literature does not provide a stability evaluation method for digitally controlled LCL filtered grid-connected inverters that accounts for computation and PWM delays, nor does it provide a general guideline for selecting controller parameters to ensure stability. In this paper, Sect. 2 introduces a typical model of an LCL filtered grid-connected inverter, and the traditional method to evaluate CCF active damping is reviewed briefly. Section 3 is devoted to a theoretical explanation of the impact of time delays on active damping and the equivalent virtual impedance caused by time delays. In Sect. 4, by using a critical value of the active damping coefficient, a stability evaluation method is developed. Necessary conditions to ensure stability, and steps for designing controller parameters to optimize the performance of active damping and dynamic response, are presented in Sect. 5. Simulation and experimental results verify the presented evaluation method in Sects. 6, and 7 concludes this paper.

2 CCF active damping in continuous domain

2.1 Modeling LCL-filtered grid-connected inverter

Figure 1 shows the topology of a three-phase inverter feeding the grid through an LCL filter, composed of the inverter-side inductor L_1, filter capacitor C, and grid-side inductor L_2. The DC-side voltage U_{dc} can be supplied by absorbing active current from the grid. The objective of the inverter is to regulate the grid-side current $i_{2\_a,b,c}$ as required. For this model all parameters of each phase are assumed symmetrical, including $i_{2\_a,b,c}$, inverter-side current $i_{1\_a,b,c}$, capacitor current $i_{C\_a,b,c}$, grid voltage $V_{g\_a,b,c}$, grid-side current $i_{g\_a,b,c}$, and local load current $i_{L\_a,b,c}$.

A block diagram of the inverter and controller is given in Fig. 2. The synchronous dq frame is particularly suitable for analysing the direct control of active and reactive current in a three-phase system. However, there are three pairs of cross-coupling terms between the d-axis and the q-axis in the block diagram, so decoupling is necessary to achieve independent control. Hence, a synthesized system is implemented in the stationary $\alpha\beta$ frame without any cross-coupling terms, while the regulation of active and reactive current remains in the synchronous dq frame [18].

In Fig. 2, i_{2d_ref} and i_{2q_ref} represent the reference values of active and reactive current, regulated by G_{id} and G_{iq} respectively. $i_{C\_\alpha,\beta}$ are feedback currents with active damping coefficient k_{damp}. Subtracting the active damping from the output of regulator, the modulation reference signal $V_{mod\_\alpha,\beta}$ will be yield. This is fed to the PWM modulator after dividing by $U_{dc}/2$ to transform into a per-unit value. While bipolar sinusoidal pulse width modulation (SPWM) is used for inverter, the transfer magnitude of the inverter bridge K_{pwm} can be approximated by $U_{dc}/2$, since the switching frequency of inverter is assumed to be sufficiently high. G_{ff} is the grid voltage feed-forward function, and in most cases, it can be simplified to 1
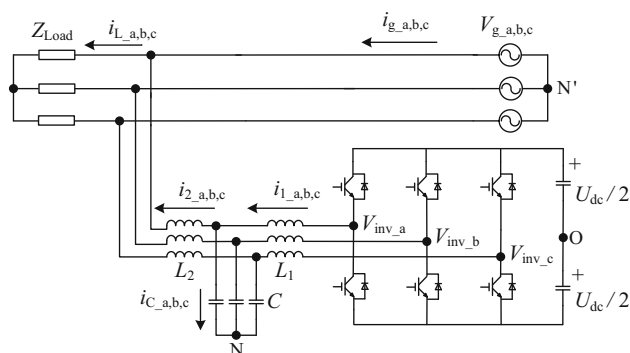
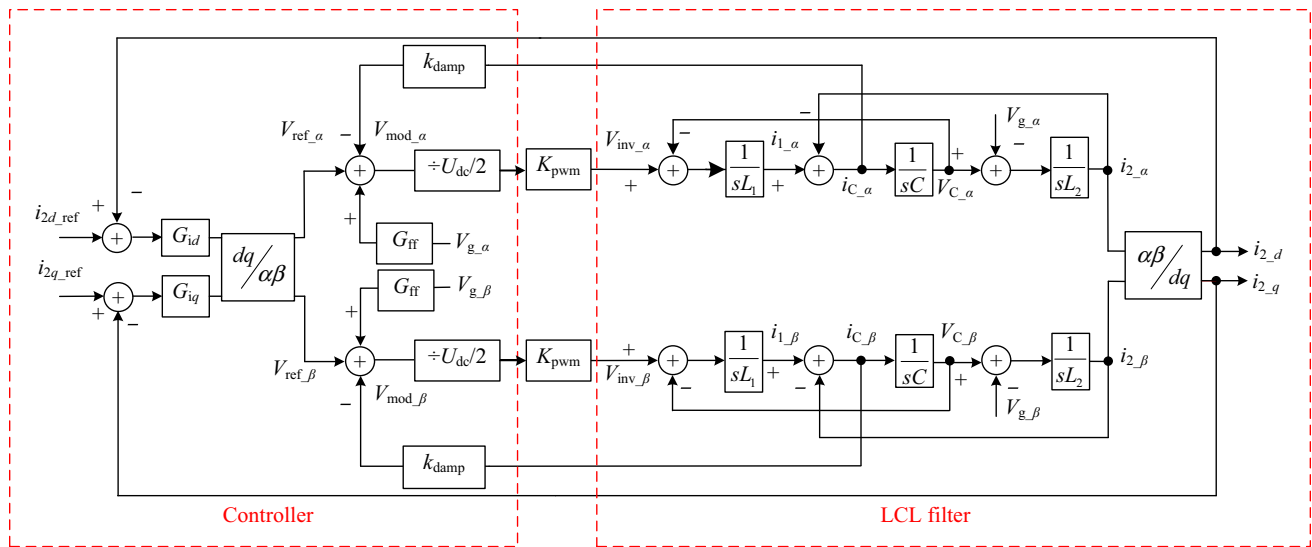**Fig. 1** Topology of a three-phase LCL filtered grid-connected inverter

Fig. 2 Synthesized system block diagram implemented in stationary $\alpha\beta$ frame and synchronous dq frame

($G_{\text{ff}} \approx 1$) when the grid voltage is mainly distorted by low-frequency harmonics [19].

For the convenience of analysis, an equivalent circuit is used for a single-phase LCL filtered grid-connected inverter, as shown in Fig. 3. R is the virtual resistor connected in parallel with filter capacitor, representing the effect of CCF active damping. V_{PCC} is the voltage at the point of common coupling of the inverter and grid.

2.2 Evaluation method of CCF active damping in continuous domain

Figure 4 shows a typical dual-loop control system with CCF via an active damping coefficient k_{damp}. The grid
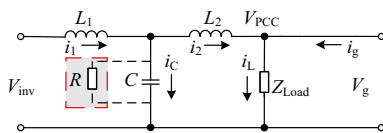

Fig. 3 Single-phase equivalent circuit of LCL filtered grid-connected inverter with virtual resistor connected in parallel with filter capacitor

voltage feed-forward function $G_{\text{ff}}(s)$ is ignored, since it has no relationship with stability. The open-loop transfer function $T_A(s)$ in the s-domain can be expressed as:

$$T_A(s) = \frac{G_i(s)}{s^3 L_1 L_2 C + s^2 L_2 C k_{\text{damp}} + s(L_1 + L_2)} \quad (1)$$

To assess the relationship between active damping and the LCL filter resonance peak, it is assumed that the current regulator gain $G_i(s) = 1$. Typically the crossover frequency f_c is restricted to be much lower than switching frequency f_{sw} (f_{sw} is equal to sampling frequency f_s) for the effectiveness of attenuating high-frequency harmonics. Although some of the latest research suggests setting the resonance frequency f_r to be higher than the Nyquist frequency $f_s/2$ [20], this is not the general practice, which regards $f_r < f_s/2$ as necessary to ensure system controllability [21].

The frequency responses of open-loop gain are depicted in Fig. 5. The dashed curve shows the case without damping, which causes a high resonance magnitude accompanied by a sharp phase transition through $-180°$, and this is an unstable situation for all controller gains. In contrast, active damping can both reduce the resonance
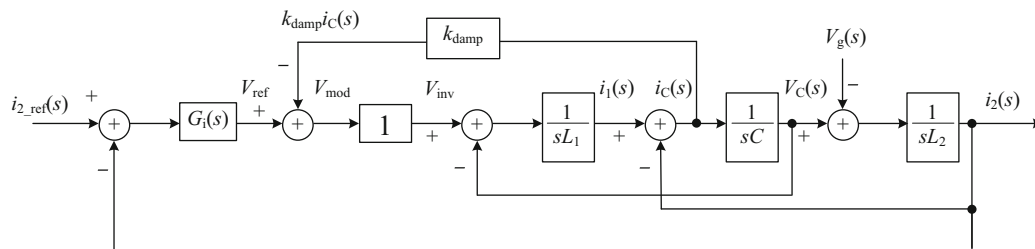

Fig. 4 Block diagram of single-phase LCL filtered grid-connected inverter with CCF active damping
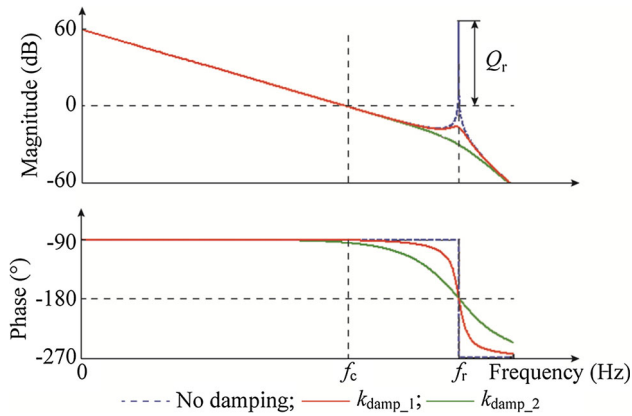
STATE GRID
STATE GRID ELECTRIC POWER RESEARCH INSTITUTE

Fig. 5 Bode diagram of CCF active damping with coefficients $k_{damp\_1} = 5$ and $k_{damp\_2} = 10$

peak magnitude and smooth the phase transition, as shown in Fig. 5 for two different damping coefficients. However, increasing k_{damp}, results in a negative phase shift for frequencies between f_c and f_r, which means an over-damped system might lead to a poor phase margin. Therefore, the system should be stabilized by a suitable damping coefficient. Damping performance is evaluated by the 'Q_r'-factor, related to the peak magnitude of the frequency response plot at the resonance frequency, such that the lower is the 'Q_r' the better is the damping performance [22].

3 Impacts on active damping caused by time delays

3.1 Modeling equivalent virtual impedance when taking time delays into account

The basic method of controller design for LCL filtered grid-connected inverter in continuous domain has been reviewed above. However, the controller is widely implemented by means of a digital micro-processor, and time delays shouldn't be omitted, so the impacts on active damping and stability should be discussed.

The detailed mechanism of time delays generated in a digitally controlled inverter has been analyzed in [15]. Taking into account one sample period (T_s) of computation delay and a half sample period ($0.5T_s$) of PWM delay, the block diagram of a digitally controlled system is introduced in Fig. 6a. Synchronous sampling is adopted in this paper, and the switching samplers are introduced into the feedback of the grid-side current, the capacitor current, and the reference value of current. The switching samplers can be represented in the s-domain by $1/T_s$ [23], and after a series of transformations the block diagram in the continuous domain is obtained as shown in Fig. 6b. The CCF active damping can be represented by a model of virtual impedance connected in parallel with the filter capacitor, the virtual impedance expresses as $Z_{eq}(s)$:
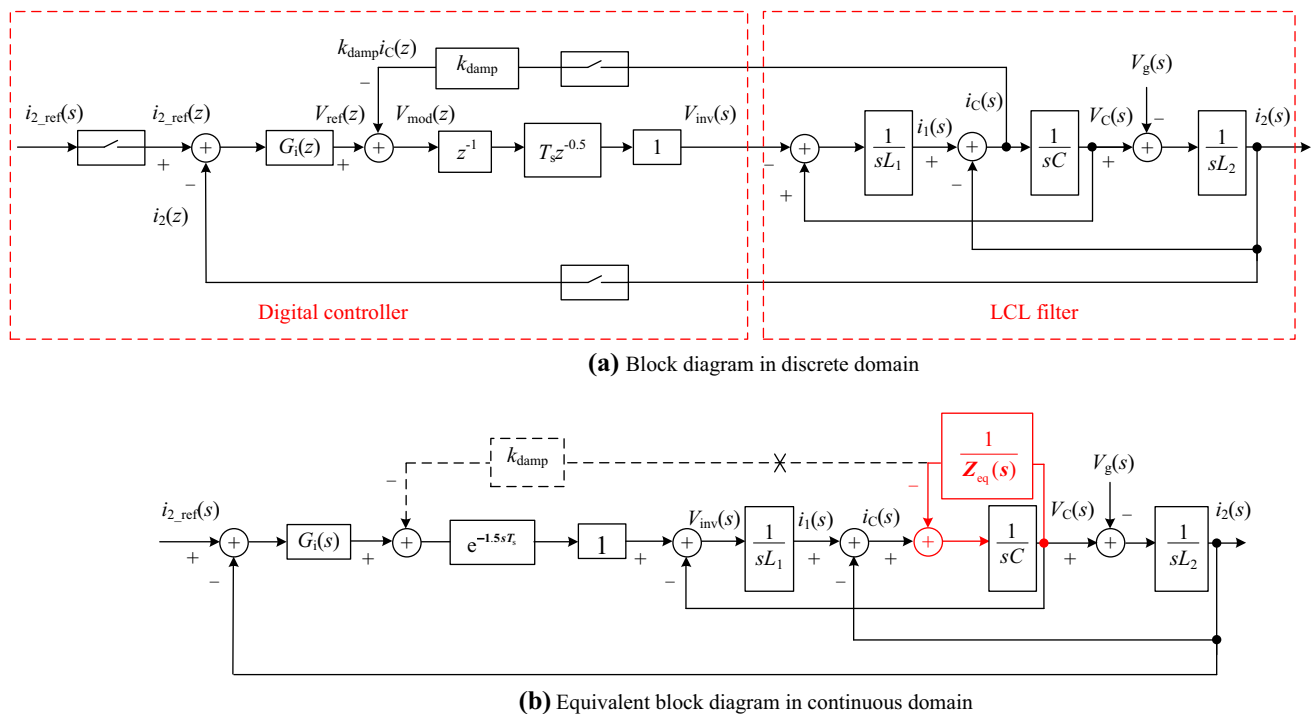

(a) Block diagram in discrete domain

(b) Equivalent block diagram in continuous domain

Fig. 6 Block diagram of a digital controlled inverter system taking time delays into account

$$Z_{eq}(s) = Re^{1.5sT_s} \triangleq R_{eq}(\omega) // jX_{eq}(\omega) \tag{2}$$

where

$$\begin{cases} R_{eq}(\omega) = \dfrac{R}{\cos(1.5\omega T_s)} = \dfrac{R}{\cos 3\pi \dfrac{f}{f_s}} \\[4mm] X_{eq}(\omega) = \dfrac{R}{\sin(1.5\omega T_s)} = \dfrac{R}{\sin 3\pi \dfrac{f}{f_s}} \end{cases} \tag{3}$$

The virtual resistor has been changed into another form of parallel connection with a resistance R_{eq} and a reactance X_{eq} [15], shown as the dashed box in Fig. 7a. Both two components are frequency dependent and have two singular points respectively ($f = f_s/6$ for R_{eq}, and $f = f_s/3$ for X_{eq}) as shown in Fig. 7b.
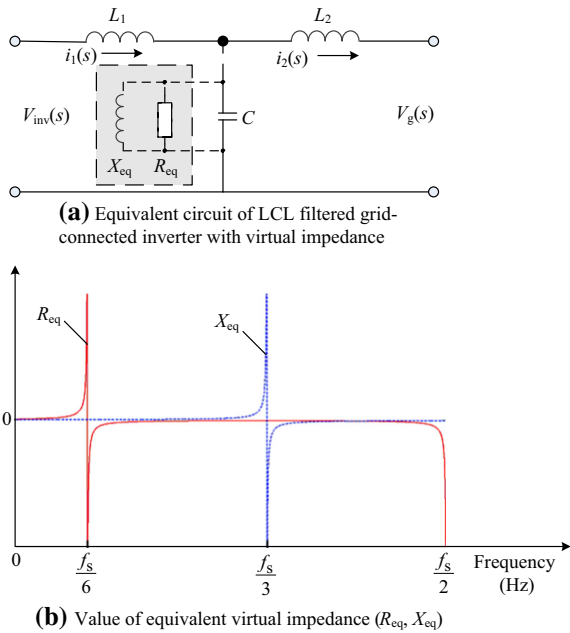

(a) Equivalent circuit of LCL filtered grid-connected inverter with virtual impedance

(b) Value of equivalent virtual impedance (R_{eq}, X_{eq})

Fig. 7 Model of equivalent virtual impedance taking $1.5T_s$ time delays into account

3.2 Impact on damping performance

The virtual reactance X_{eq} is inductive when $f \in (0, f_s/3)$, but capacitive when $f \in (f_s/3, f_s/2)$. This changes the effective value of the filter capacitor. And according to (4) the resonance frequency f_r will then be shifted to a new one f_r'.

$$f_r = \frac{\omega_r}{2\pi} = \frac{1}{2\pi}\sqrt{\frac{L_1 + L_2}{L_1 L_2 C}} \tag{4}$$

For instance, in the range of $(0, f_s/3)$, X_{eq} yields a higher resonance frequency f_r' because of the effective value of filter capacitor is decreased; conversely, in the range of $(f_s/3, f_s/2)$, X_{eq} yields a lower f_r'. Whether decreased or increased, f_r' will only approach but never step over $f_s/3$, the singular point of X_{eq}.

Generally, in order to damp a resonance peak, positive R_{eq} is required, which occurs when $f \in (0, f_s/6)$. But R_{eq} is negative when $f \in (f_s/6, f_s/2)$, and even worse, R_{eq} approaches infinity when $f = f_s/6$, in other words, the resistance approaches an open circuit state (no damping) at the singular point of $f_s/6$.

Table 1 summarises the behaviour of X_{eq} and R_{eq} and their impacts on resonance frequency and active damping. These impacts mean that evaluating stability and selecting active damping parameters in a digital controller are completely different from the conventional situation in the continuous domain, due to the effect of time delays.

4 Evaluation method of stability regarding time delays

4.1 Descriptions of Nyquist stability criterion

The Nyquist stability criterion is widely used for designing and analyzing linear and time-invariant systems with feedback, and it is adopted in this paper. Before evaluating stability, the significance of $-180°$ phase crossings within the frequency ranges that have magnitudes

Table 1 Detailed analysis of impacts on virtual impedance

Working frequency f	X_{eq}		R_{eq}	
	State	Impact on resonance frequency	State	Impact on active damping
$(0, f_s/6)$	Inductive	f_r is increased to a higher f_r'	Positive	Beneficial effect on f_r' when $f_r' \in (0, f_s/6)$
$f_s/6$			Infinity	No contribution when $f_r' = f_s/6$
$(f_s/6, f_s/3)$			Negative	Adverse effect on f_r' when $f_r' \in (f_s/6, f_s/2)$
$f_s/3$	Infinity	f_r' will never step over $f_s/3$		
$(f_s/3, f_s/2)$	Capacitive	f_r is decreased to a lower f_r'		

above 0 dB in bode diagram, and their relationship with open-loop unstable poles, should be reviewed as follows:

1) A $-180°$ crossing where phase increases with frequency is defined as positive crossing; a $-180°$ crossing where phase decreases with frequency is defined as negative crossing. The numbers of positive and negative crossings are denoted by C^+ and C^- respectively.

2) The value of $2(C^+ - C^-)$ must be equal to the number of open-loop unstable poles to ensure stability. If no open-loop unstable pole exists, that means the value of $2(C^+ - C^-)$ must be equal to zero to ensure stability, so the value of C^+ also should be equal to zero, since C^- is restricted to zero by the Nyquist criterion; if a pair of open-loop unstable poles exists, that means the value of $2(C^+ - C^-)$ must be equal to 2 to ensure stability, so the value C^+ should be equal to 1.

4.2 Location of unstable open-loop poles

Based on the equivalent block diagram of the system in continuous domain shown in Fig. 6b, the open-loop gain with time delays can be easily derived, and is shown in (5). The denominator of $T_{A\_Delay}(s)$ contains a nonlinear element $e^{-1.5sT_s}$, a transcendental function with open-loop poles that cannot be solved directly in the s-domain. On the other hand, $T_D(z)$ can be derived from Fig. 6a as the discrete representation of open-loop gain, an expression without any nonlinear element in the denominator part as shown in (6), and this form is preferred for determining poles. Thus, unstable open-loop poles can be comprehensively explored in the z-plane.

$$T_{A\_Delay}(s) = \frac{G_i(s)e^{-1.5sT_s}}{s^3 L_1 L_2 C + s^2 L_2 C k_{damp} e^{-1.5sT_s} + s(L_1 + L_2)}$$

(5)

$$T_D(z) = \frac{G_i(z)}{\omega_r(L_1 + L_2)} \cdot$$

$$\frac{\omega_r T_s(z^2 - 2z\cos(\omega_r T_s) + 1) - (z-1)^2 \sin(\omega_r T_s)}{(z-1)\left[z(z^2 - 2z\cos(\omega_r T_s) + 1) + (z-1)\frac{k_{damp}\sin(\omega_r T_s)}{\omega_r L_1}\right]}$$

(6)

A critical value of the active damping coefficient k_{damp_c} is proposed as shown in (7). The relationship between k_{damp_c}, the ratio of resonance frequency to sampling frequency f_r/f_s, and the sampling frequency f_s is depicted by Fig. 8. Parameters $f_s = 10$ kHz and $L_1 = 2.3$ mH are used as a typical example. The resonance frequency can be divided into three regions depending on $k_{damp\_c} > 0$, $k_{damp\_c} = 0$, and $k_{damp\_c} < 0$, defined as low resonance
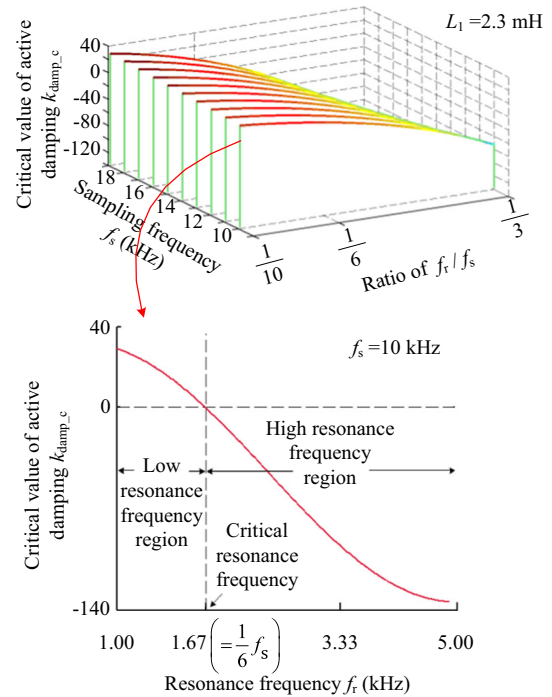

Fig. 8 Variation of critical value k_{damp_c} with sampling frequency f_s and resonance frequency f_r

frequency region, critical resonance frequency, and high resonance frequency region.

$$k_{damp\_c} = \frac{\left[2\cos\left(2\pi\frac{f_r}{f_s}\right) - 1\right]2\pi f_r L_1}{\sin\left(2\pi\frac{f_r}{f_s}\right)}$$

(7)

The location of unstable open-loop poles can be easily concluded by means of k_{damp_c}:

1) If $k_{damp} > k_{damp\_c}$, there is a pair of unstable open-loop poles, and when $k_{damp} < k_{damp\_c}$, no unstable open-loop poles exist. Substituting $k_{damp} = k_{damp\_c}$ into $T_D(z)$ allows a pair of critical open-loop poles $z_{1,2} = (1 \pm j\sqrt{3})/2$ to be calculated, located on the unit circle of z-plane. Their unique mapping poles $s_{1,2} = \pm j\pi f_s/3$ (related to the frequency $f_s/6$) on the imaginary axis of s-plane can also be exactly derived.

2) The magnitude of $T_D(z)\|_{z=e^{-j\pi/3}}$ tends towards infinity, yielding a new resonance frequency of $f_s/6$. This is defined as the critical resonance frequency, where the $-180°$ crossing definitely will occur in bode diagram.

4.3 Stability evaluation method

Based on the previous analysis, the stability evaluation can be focused on the relationship between k_{damp} and k_{damp_c}. When the value of k_{damp_c} is different from the

Table 2 Regions and sub-cases in stability analysis

Value of k_{damp_c}	Resonance frequency	Sub-cases
$k_{damp\_c} > 0$	$f_r < f_s/6$	1.1 $k_{damp} > k_{damp\_c} > 0$
		1.2 $k_{damp} = k_{damp\_c} > 0$
		1.3 $0 < k_{damp} < k_{damp\_c}$
$k_{damp\_c} = 0$	$f_r = f_s/6$	2.1 $k_{damp} > 0$
		2.2 $k_{damp} = 0$
$k_{damp\_c} < 0$	$f_s/6 < f_r < f_s/2$	3.1 $k_{damp} > 0 > k_{damp\_c}$
		3.2 $k_{damp} = 0 > k_{damp\_c}$

resonance frequency, the problem should be divided into three regions, and each region has sub-cases as listed in Table 2. Each sub-case will now be discussed.

Case 1.1: If $k_{damp} > k_{damp\_c} > 0$, the resonance frequency is located in the low region ($f_r < f_s/6$), and $k_{damp\_c} > 0$ is satisfied, so a pair of open-loop unstable poles is produced. Hence, to ensure stability, the value of $2(C^+ - C^-)$ must be equal to 2, i.e., $C^+ = 1$ and $C^- = 0$, which means the positive $-180°$ crossing should be at $f_s/6$. Consequently, the magnitude margin at f_r defined as GM_1 must be greater than 0 dB to prevent the negative crossing, i.e. $C^- = 0$; and the magnitude margin at $f_s/6$ defined as GM_2 must be smaller than 0 dB to ensure the positive crossing, i.e. $C^+ = 1$. The bode diagram for this case is shown in Fig. 9a.

The resonance frequency is shifted to a higher one ($f_r' > f_s/6$), and as discussed in Sect. 3.2 the virtual resistance R_{eq} is negative and has adverse effect on active damping when $f_r' \in (f_s/6, f_s/2)$. The stringent constraint on overall stability margins is an adverse effect of negative R_{eq}.

Case 1.2: If $k_{damp} = k_{damp\_c} > 0$ while $f_r < f_s/6$, $k_{damp\_c} > 0$ is satisfied and a pair of open-loop poles arises on the imaginary axis of s-plane. According to the previous analysis, the critical resonance peak is shifted to $f_s/6$ ($f_r' = f_s/6$). Although active damping fails to suppress the resonance peak, the system can remain stable when the value of $2(C^+ - C^-)$ remains 0, i.e. when $C^+ = 0$ and GM_1 is greater than 0 dB. The bode diagram is shown in Fig. 9b.

A critical resonance peak is produced but cannot be damped when $k_{damp} = k_{damp\_c}$, and the virtual resistance R_{eq} approaches an open-circuit state at the singular point of $f_s/6$, which means R_{eq} makes no contribution to suppression when the resonance peak is located at critical resonance frequency.

Case 1.3: If $0 < k_{damp} < k_{damp\_c}$ while $f_r < f_s/6$, $k_{damp\_c} > 0$ is satisfied, and no unstable pole exists. Hence, GM_1 greater than 0 dB and $C^- = 0$ is enough for ensuring stability. The bode diagram is shown in Fig. 9c.

The resonance frequency $f_r' \in (0, f_s/6)$ so the virtual resistance R_{eq} is positive and has beneficial effect on active damping. The relaxed stability condition is seemed as the beneficial effect from positive R_{eq}.

Case 2.1: If $k_{damp} > k_{damp\_c} = 0$ and the resonance frequency is located at the critical point ($f_r = f_s/6$), $k_{damp\_c} = 0$ is satisfied, and a pair of open-loop unstable poles is produced. Similarly to the Case 1.1, negative and positive crossings should occur at f_r and $f_s/6$ respectively, which causes the phase-frequency curve to touch the scale line of $-180°$ in the bode diagram, i.e. $C^+ = 0.5$. The system cannot be stable irrespective of active damping. The bode diagram is shown in Fig. 9d.

Case 2.2: If $k_{damp} = k_{damp\_c} = 0$ and $f_r = f_s/6$, $k_{damp\_c} = 0$ is satisfied. The system is unstable with no damping supplied for the resonance peak and the negative crossing occurs at the critical resonance frequency.

Case 3.1: If $k_{damp} > 0 > k_{damp\_c}$ while the resonance frequency is located in the high region ($f_s/6 < f_r < f_s/2$), $k_{damp\_c} < 0$ is satisfied and a pair of open-loop unstable poles is produced, similarly to Case 1.1. It should be noted that the frequency of positive crossing is changed to f_r, so the necessary magnitude margins are $GM_2 > 0$ dB to prevent the negative crossing at $f_s/6$, i.e. $C^- = 0$, and $GM_1 < 0$ dB to ensure the positive crossing, i.e. $C^+ = 1$. The bode diagram is shown in Fig. 9e.

Case 3.2: If $k_{damp} = 0 > k_{damp\_c}$ while $f_s/6 < f_r < f_s/2$, $k_{damp\_c} < 0$ is satisfied, and this case is shown by the dashed curve (no damping) in Fig. 9e. Here it can be seen that the phase transits below $-180°$ at $f_s/6$ (well before the resonance frequency), which means, even though there is no damping to supress the resonance peak, the system is naturally stabilized by selecting a suitable gain for the current regulator, because the magnitude response crosses 0 dB prior to $f_s/6$. An updated bode diagram with no damping is shown in Fig. 9f, where the current regulator gain of G_{i1} is larger than G_{i2}. The magnitude margin at $f_s/6$ defined as $GM2_{Nodamping}$ must be greater than 0 dB to ensure stability.

This analysis leads to a generalized stability evaluation method accounting for digital controller time delays, as follows:

1) If $k_{damp\_c} > 0$, which is equivalent to the condition that the LCL resonance frequency is in the low region ($f_r < f_s/6$), $k_{damp} > 0$ is necessary for stability so active damping is applied. A sufficient but smaller damping coefficient ($k_{damp} < k_{damp\_c}$) is recommended as an optimal solution because the virtual resistance R_{eq} makes a contribution to active damping. In contrast,
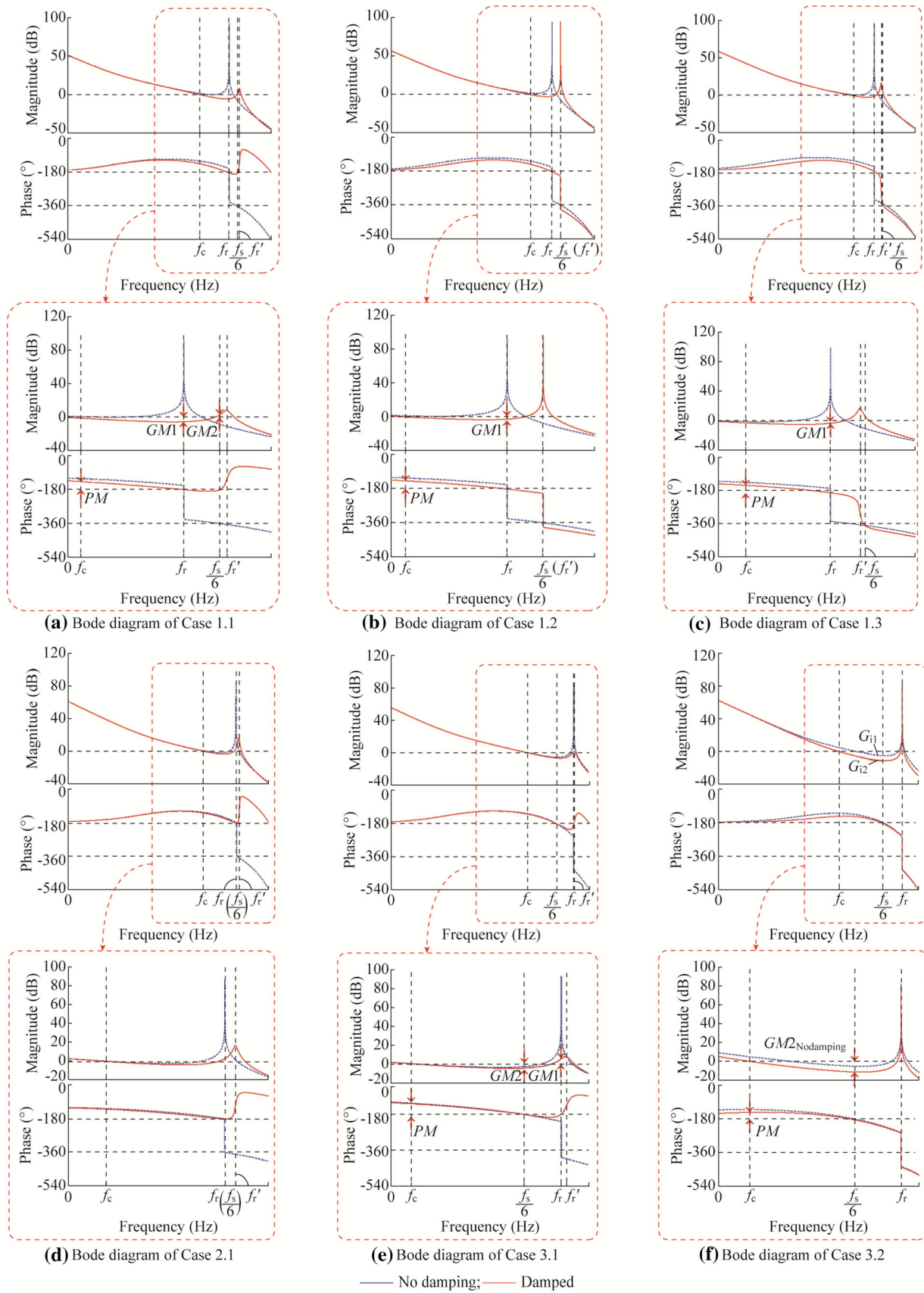
(a) Bode diagram of Case 1.1

(b) Bode diagram of Case 1.2

(c) Bode diagram of Case 1.3

(d) Bode diagram of Case 2.1

(e) Bode diagram of Case 3.1

(f) Bode diagram of Case 3.2

—— No damping; —— Damped

Fig. 9 Bode diagram of sub-cases of stability analysis

over damping ($k_{\mathrm{damp}} > k_{\mathrm{damp\_c}}$) leads to an adverse effect, and the conditions of overall stability would be compromised. The critical damping ($k_{\mathrm{damp}} = k_{\mathrm{damp\_c}}$) solution should be avoided because it leads to a new resonance frequency ($f_{\mathrm{s}}/6$), where R_{eq} makes no contribution to damping the resonance peak.

2) If $k_{\mathrm{damp\_c}} = 0$, which is equivalent to the condition that the LCL resonant frequency is equal to the critical frequency ($f_{\mathrm{s}}/6$), the system will be unstable irrespective of active damping, unless additional modifications are implemented to the controller time delays [15].

3) If $k_{\mathrm{damp\_c}} < 0$, which is equivalent to the condition that LCL resonant frequency is above the critical frequency ($f_{\mathrm{s}}/6 < f_{\mathrm{r}} < f_{\mathrm{s}}/2$), and even if $k_{\mathrm{damp}} = 0$ a single loop of grid-side current feedback is naturally stabilized by a proper current regulator gain. Certainly, system is also stable when a redundant damping solution ($k_{\mathrm{damp}} > 0$) is applied.

Therefore, $k_{\mathrm{damp\_c}}$ is an important measure of stability and $k_{\mathrm{damp\_c}} = 0$ will cause instability.

5 Design method for controller parameters

5.1 Phase and magnitude margins

High-performance LCL filtered grid-connected converters should have fast dynamic response, sufficient switching frequency attenuation, and good damping performance while preserving stability. This section provides guidelines for selecting controller parameters. A proportional integral (PI) current regulator is adopted in this paper, which expresses as $G_{\mathrm{i}}(s) = K_{\mathrm{p}} + K_{\mathrm{i}}/s$.

Dynamic response is mainly evaluated by the phase margin (PM) at the unity-gain crossover frequency f_{c}, and as discussed above, to guarantee the robust stability of system, sufficient magnitude margins $GM1$ and $GM2$ also should be assured. PM, $GM1$ and $GM2$ are deduced and presented from (8) to (10). $PM_{\mathrm{Nodamping}}$ and $GM2_{\mathrm{Nodamping}}$ can be derived by substituting $k_{\mathrm{damp}} = 0$ into (8) and (10). Typically, $PM \in (30°, 60°)$, and $3 < |GM| < 6$ are recommended to ensure satisfactory dynamic response and robust stability [24].

$$
\begin{aligned}
PM &= 180° + \angle T_{\mathrm{A\_Delay}}(s)\big|_{s=\mathrm{j}2\pi f_{\mathrm{c}}} \\
&= \arctan\frac{2\pi f_{\mathrm{c}}K_{\mathrm{p}}}{K_{\mathrm{i}}} - 3\pi\frac{f_{\mathrm{c}}}{f_{\mathrm{s}}} \\
&\quad - \arctan\frac{f_{\mathrm{c}}k_{\mathrm{damp}}\cos\left(3\pi\frac{f_{\mathrm{c}}}{f_{\mathrm{s}}}\right)}{f_{\mathrm{c}}k_{\mathrm{damp}}\sin\left(3\pi\frac{f_{\mathrm{c}}}{f_{\mathrm{s}}}\right) + 2\pi L_1\left(f_{\mathrm{r}}^2 - f_{\mathrm{c}}^2\right)}
\end{aligned} \tag{8}
$$

$$
\begin{aligned}
GM1 &= -20\lg\left|T_{\mathrm{A\_Delay}}(s)\right|\big|_{s=\mathrm{j}2\pi f_{\mathrm{r}}} \\
&= -20\lg\left|\frac{K_{\mathrm{p}}L_1}{k_{\mathrm{damp}}(L_1 + L_2)}\right|
\end{aligned} \tag{9}
$$

$$
\begin{aligned}
GM2 &= -20\lg\left|T_{\mathrm{A\_Delay}}(s)\right|\big|_{s=\mathrm{j}2\pi\frac{f_{\mathrm{s}}}{6}} \\
&= -20\lg\left|\frac{K_{\mathrm{p}}}{\frac{\pi}{3}f_{\mathrm{s}}L_1L_2C\left[(2\pi f_{\mathrm{r}})^2 - \left(\frac{\pi}{3}f_{\mathrm{s}}\right)^2 + \frac{\pi}{3}f_{\mathrm{s}}\frac{k_{\mathrm{damp}}}{L_1}\right]}\right|
\end{aligned} \tag{10}
$$

5.2 Selection of optimum damping parameters

The selection of k_{damp} directly impacts the performance of active damping. In order to demonstrate the selection of optimum damping parameters, two typical design examples with different LCL filters are given in Table 3. For these two designs, Fig. 10 shows the variation of 'Q_{r}'-factor with different k_{damp}.

For example filter 1, $k_{\mathrm{damp\_c}} > 0$, while the resonance frequency is located in the low region ($f_{\mathrm{r}} = 1.40$ kHz). As seen in Fig. 10a, the value of Q_{r} is high if active damping is not supplied ($k_{\mathrm{damp}} = 0$), or if the damping coefficient is equal to the critical value ($k_{\mathrm{damp}} = k_{\mathrm{damp\_c}} = 7.2$), so that active damping fails to suppress the resonance peak. In contrast, Q_{r} approaches 0 dB by selecting a damping coefficient higher than 4, and thus optimum damping performance could be achieved by $k_{\mathrm{damp}} = 4$. Similarly, $k_{\mathrm{damp}} = 10$ could be chosen for an over-damped solution, and then Q_{r} is less than 0 dB.

Table 3 Parameter list of typical examples

Nominal system parameters	$V_{\mathrm{g}} = 220$ V
	50 Hz
	$U_{\mathrm{dc}} = 800$ V
	$f_{\mathrm{s}} = 10$ kHz
	$T_{\mathrm{s}} = 100$ μs
	$f_{\mathrm{s}}/6 = 1.67$ kHz
	$f_{\mathrm{s}}/2 = 5$ kHz
Filter 1	$L_1 = 2.3$ mH
($f_{\mathrm{r}} = 1.40$ kHz)	$L_2 = 0.9$ mH
	$C = 20$ μF
	$f_{\mathrm{c}} = 0.5$ kHz
	$k_{\mathrm{damp\_c}} = 7.2$
Filter 2	$L_1 = 1$ mH
($f_{\mathrm{r}} = 2.34$ kHz)	$L_2 = 0.3$ mH
	$C = 20$ μF
	$f_{\mathrm{c}} = 0.5$ kHz
	$k_{\mathrm{damp\_c}} = -11.8$

Fig. 10 Variation of 'Q_r'-factor with different k_{damp}

Table 4 Optimized controller parameters of typical examples

Filter	Cases	Parameters
Filter 1	Over damping solution (Case 1.1)	$k_{damp} = 10$ $K_p = 9$ $K_i = 1000$ $f_r' = 1.77$ kHz $PM = 54°$ $GM1 = 4.0$ dB $GM2 = -4.2$ dB
	Critical damping (Case 1.2)	$k_{damp} = 7.2$ $K_p = 5$ $K_i = 1000$ $f_r' = 1.67$ kHz $PM = 65°$ $GM1 = 6.3$ dB
	Optimum damping solution (Case 1.3)	$k_{damp} = 4$ $K_p = 4$ $K_i = 1000$ $f_r' = 1.55$ kHz $PM = 61°$ $GM1 = 6.4$ dB
Filter 2	Redundant damping solution (Case 3.1)	$k_{damp} = 2$ $K_p = 5$ $K_i = 500$ $f_r' = 2.46$ kHz $PM = 50°$ $GM1 = -5.8$ dB $GM2 = 4.2$ dB
	No damping solution (Case 3.2)	$k_{damp} = 0$ $K_p = 3$ $K_i = 500$ $PM_{NoDamping} = 62°$ $GM2_{NoDamping} = 7.2$ dB

For example filter 2, $k_{damp\_c} < 0$, while the resonance frequency is located in the high region ($f_r = 2.34$ kHz). As mentioned at the end of Sect. 4.3, a single loop of grid-side current feedback without damping can sometimes be stabilized, but, as seen in Fig. 10b, the high Q_r when $k_{damp} = 0$ indicates that the resonance peak still exists. Moreover, Q_r does not show any significant improvement beyond $k_{damp} = 2$, so $k_{damp} = 2$ is considered as the redundant damping solution.

The optimized controller parameters for these two examples, including PI regulators, active damping parameters and stability margins, are presented in Table 4.

5.3 Root loci

After exploring stability margins using bode diagram to ensure all the parameters above are selected correctly, it is also necessary to investigate the movement of closed-loop transfer function poles by root loci to verify the stable operating region.

For example filter 1, Fig. 11a shows the root loci of variation in active damping parameter for the PI regulator. By increasing k_{damp} from zero, the dominant poles will be forced to track back inside the unit circle, and the overall system becomes stable. However, the over-damping ($k_{damp} > -k_{damp\_c}$) solution will make the poles track back outside the unit circle, thus, stability will deteriorate. The part of the root loci within the unit circle boundary region determines the upper and lower limit of k_{damp}, so the observation of root loci verifies the value of k_{damp} calculated for filter 1 in Table 4.

For example filter 2, Fig. 11b shows the root loci of variation in proportional gain for the single-loop system without active damping. The dominant poles track well inside the unit circle, hence, the system remains stable until K_p becomes larger than the upper limit. The observation of root loci also verifies the result of K_p calculated for filter 2 in Table 4.

Figure 11c shows the root loci of variation in k_{damp} when $k_{damp\_c} = 0$, while the resonance frequency is close to the critical resonance frequency. As can be seen, the system will be unstable irrespective of active damping.

6 Verification of evaluation method

6.1 Verification by simulation

Using the parameters in Table 4, both simulations and experiments were performed on a three-phase distribution

(a) Root loci with a variable k_{damp} when $k_{damp} > 0$

(b) Root loci with no damping when $K_{damp\_c} < 0$

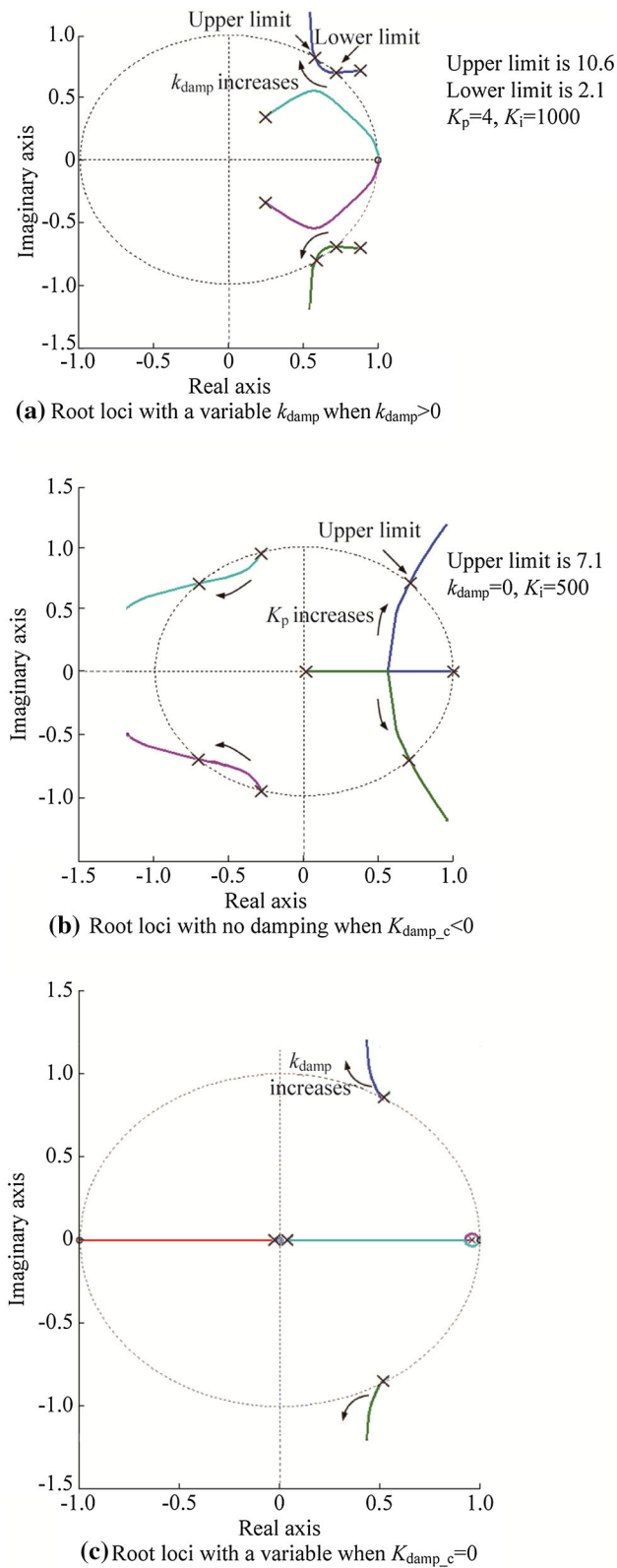**(c)** Root loci with a variable when $K_{damp\_c} = 0$

Fig. 11 Root loci

static compensator (D-STATCOM). Simulations were implemented to verify the stability evaluation method and the guidelines for controller design, examining the effect of harmonic attenuation, the dynamic response, and the performance of active damping.

The primary objective of the D-STATCOM is to regulate the grid-side current i_2 as the reactive load requires. The control algorithm is implemented in a synthesized scheme including a stationary $\alpha\beta$ frame and a synchronous dq frame. Reference values of reactive current i_{2q} stepping from 30 to 15 A were examined to evaluate the transient response.

Simulation results with example filter 1 are shown in Fig. 12a–c.

The reference current steps down at 0.1 s, and the converter operates without oscillation with active damping is enabled. Active damping is disabled at 0.2 s, and immediately a large resonant current arises for all three cases. It is clear that active damping is necessary to maintain stability when $k_{damp\_c} > 0$. Moreover, a fast Fourier transform (FFT) of the grid-side current demonstrates the effectiveness of the filter. Compared with the over-damping solution in Fig. 12a, a sufficient but smaller active damping ($k_{damp} < k_{damp\_c}$), i.e. an optimum solution in Fig. 12c, possesses the same total harmonic distortion (THD) and equivalent damping performance at the new resonance frequency f_r', but also achieves a faster transient response because of the enhanced phase margin. As to critical damping ($k_{damp} = k_{damp\_c}$), a significant resonant component is observed at $f_s/6$ in Fig. 12b, due to the matching condition of k_{damp}, that results in active damping being ineffective on the resonance peak.

Simulation results with filter 2 are shown in Fig. 12a–b, and both the transient response and THD are acceptable. Even without active damping, the system is still quite stable, that means active damping is not a necessary condition for LCL filtered converters when $k_{damp\_c} < 0$.

It should be noted that an abundant resonant component can be observed when there is no damping. In contrast, the redundant adoption of active damping leads to a reduced resonant component. Furthermore, comparison stability tests with different regulator gains were conducted to validate the understanding of root loci for single-loop grid-side current feedback without active damping, shown in Fig. 11b. It was discussed earlier that very high loop gain is difficult to achieve because system becomes unstable beyond a certain stage, and this is verified by Fig. 13c which shows that without active damping the stability degrades for a higher K_p close to upper limit ($K_p = 7.1$).
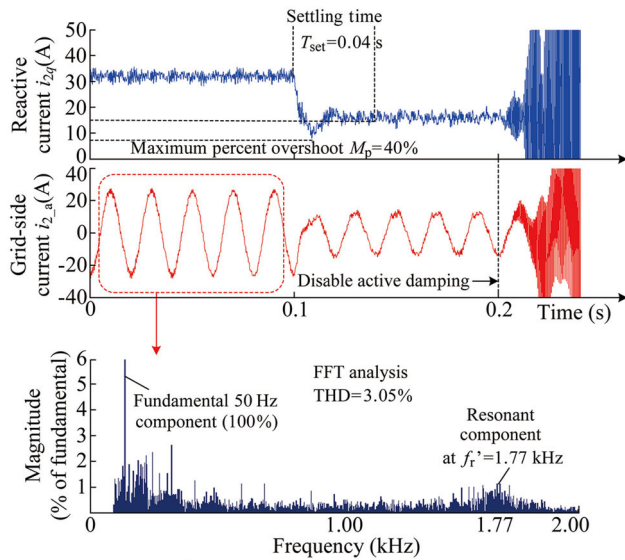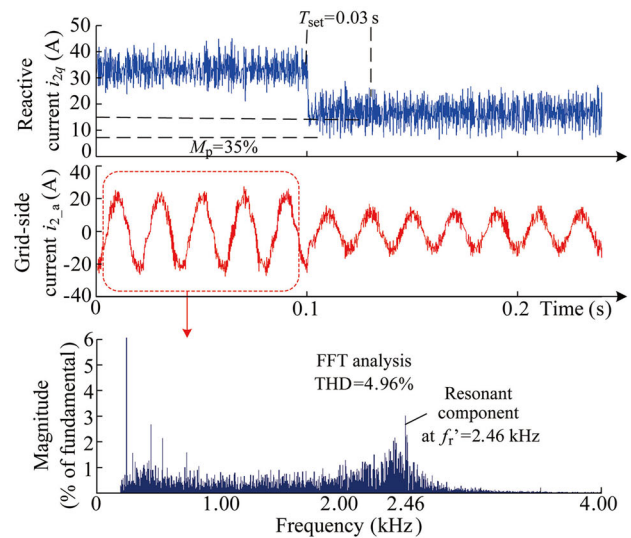
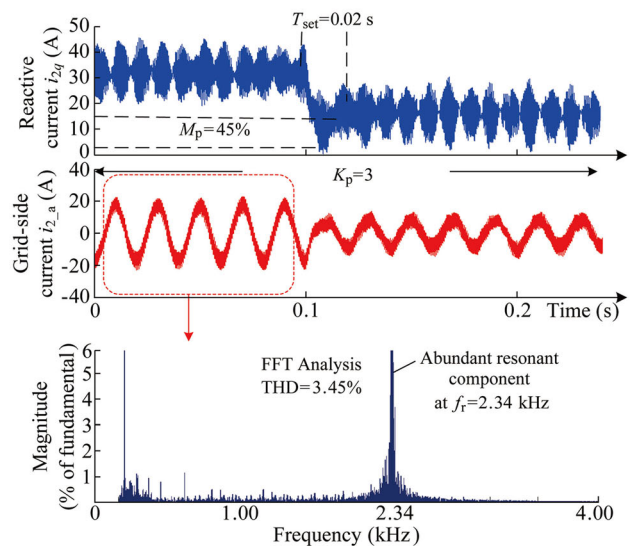(a) Results of over damping solution
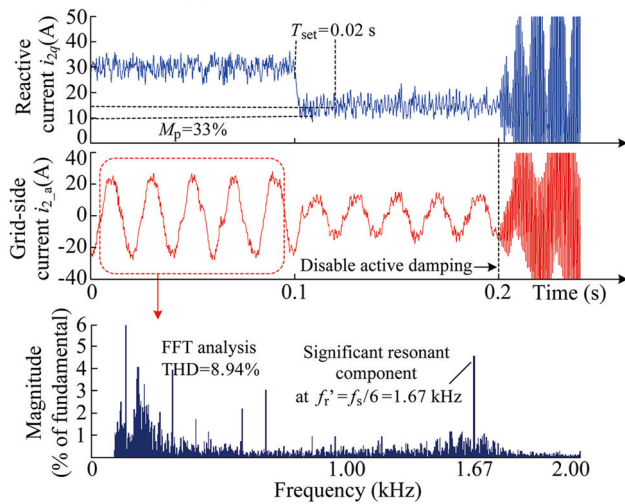
(b) Results of critical damping
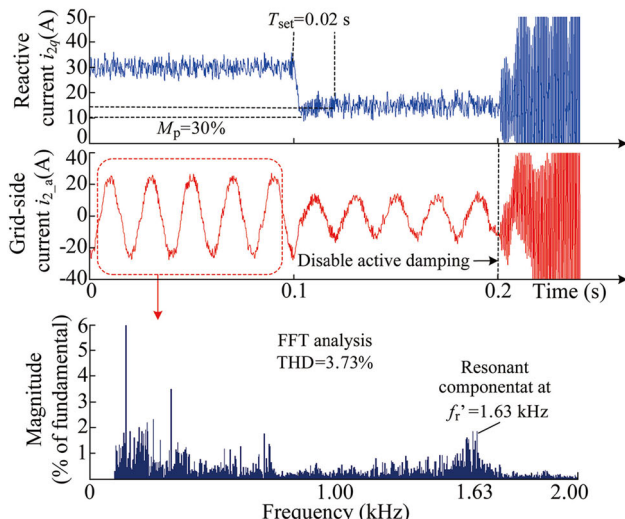
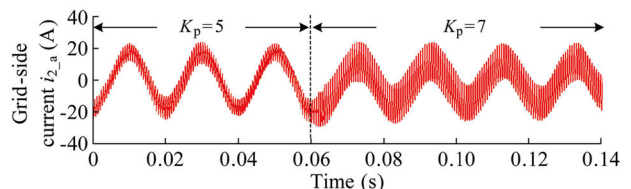(c) Results of optimum damping solution

Fig. 12 Transient response of regulated reactive current and FFT of grid-side current with filter 1 ($k_{damp\_c} > 0$)

(a) Results of redundant damping solution

(b) Results of no damping solution

(c) Test of no damping solution with different regulator gain

Fig. 13 Transient response of regulated reactive current and FFT of grid-side current with filter 2 ($k_{damp\_c} < 0$), and test of stability margin for different regulator gain when using no damping

6.2 Experimental verification

The experimental verification was carried out in three steps: ① testing the current tracking capability of the over damping solution and the optimum damping solution when using filter 1; ② testing the current tracking capability of the redundant damping solution and without damping when
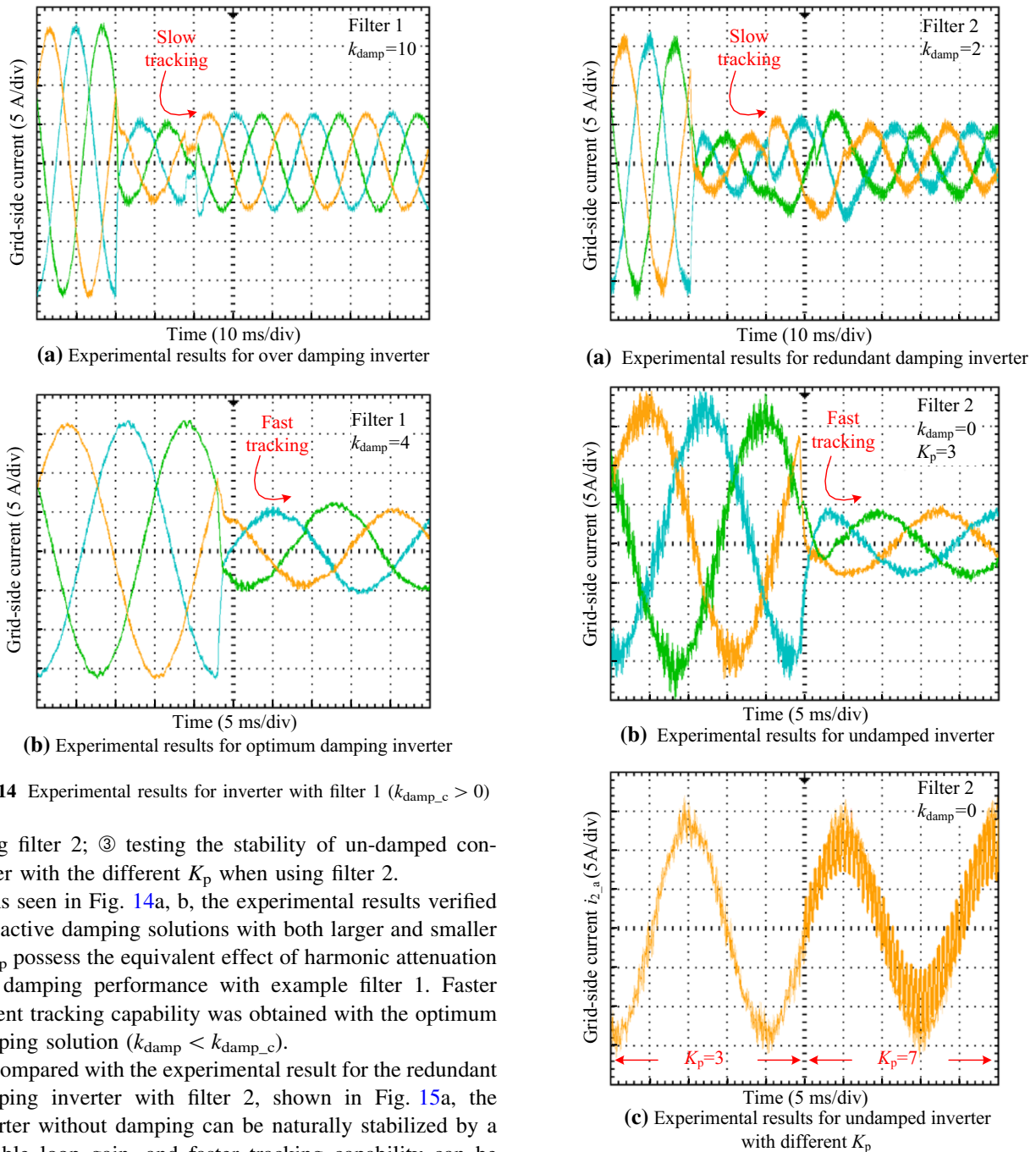
(a) Experimental results for over damping inverter

(b) Experimental results for optimum damping inverter

Fig. 14 Experimental results for inverter with filter 1 ($k_{\mathrm{damp\_c}} > 0$)

using filter 2; ③ testing the stability of un-damped converter with the different K_{p} when using filter 2.

As seen in Fig. 14a, b, the experimental results verified that active damping solutions with both larger and smaller k_{damp} possess the equivalent effect of harmonic attenuation and damping performance with example filter 1. Faster current tracking capability was obtained with the optimum damping solution ($k_{\mathrm{damp}} < k_{\mathrm{damp\_c}}$).

Compared with the experimental result for the redundant damping inverter with filter 2, shown in Fig. 15a, the inverter without damping can be naturally stabilized by a suitable loop gain, and faster tracking capability can be obtained, as shown in Fig. 15b. However, the resonance oscillation is barely suppressed when $k_{\mathrm{damp}} = 0$, and in fact the LCL filter with a high resonant frequency approaches the performance of a single L filter, hence, the benefit of having a three-order filter is lost to a large extent.

Figure 15c demonstrates that with the undamped solution it is difficult to achieve both very high loop gain and sufficient stability margins. The stability deteriorates when $K_{\mathrm{p}} = 7$. Generally, it is preferable for the controller to have wider stability margins rather than a large K_{p}.

(a) Experimental results for redundant damping inverter

(b) Experimental results for undamped inverter

(c) Experimental results for undamped inverter with different K_{p}

Fig. 15 Experimental results for inverter with filter 2 ($k_{\mathrm{damp\_c}} < 0$)

Finally, both of simulation and experimental results show an evident steady-state error. This paper is focussed on the stability evaluation method considering the stability margins and the performance of active damping, and not on minimising steady-state error, which might be effectively compensated by a fundamental proportional resonant (PR) regulator [25].

7 Conclusion

In this paper, a critical value of the CCF active damping coefficient $k_{\mathrm{damp\_c}}$ is proposed to construct a stability evaluation method for LCL filtered grid-connected converters. This value is based on analysis of the inherent relationship between time delays in the digital controller and stability. If $k_{\mathrm{damp\_c}} > 0$, while the resonance frequency is located in the low region ($f_r < f_s/6$), active damping is identified as an essential factor for stability, furthermore, a sufficient but smaller damping coefficient ($k_{\mathrm{damp}} < k_{\mathrm{damp\_c}}$) is recommended as optimum solution. In contrast, over damping ($k_{\mathrm{damp}} > k_{\mathrm{damp\_c}}$) leads to a stringent constraint on overall stability margins, and selection of critical damping ($k_{\mathrm{damp}} = k_{\mathrm{damp\_c}}$) should be avoided, because it results in a new resonance peak at the critical frequency ($f_s/6$) which cannot be damped. If $k_{\mathrm{damp\_c}} = 0$, while the resonance frequency meets the critical frequency, system will be unstable irrespective of active damping. If $k_{\mathrm{damp\_c}} < 0$, active damping is not required, and by adopting a suitable regulator gain, a single-loop controller without any additional damping is sufficient to design a stable system. Both simulation and experimental results have confirmed the stability evaluation method and verified the guidelines for selecting controller parameters to improve the stability margins and the performance of active damping.

References

[1] Li Y, Nejabatkhah F (2014) Overview of control, integration and energy management of microgrids. J Mod Power Syst Clean Energy 2(3):212–222. doi:10.1007/s40565-014-0063-1

[2] Luo A, Xu Q, Ma F et al (2016) Overview of power quality analysis and control technology for the smart grid. J Mod Power Syst Clean Energy 4(1):1–9. doi:10.1007/s40565-016-0185-8

[3] Alzola RP, Liserre M, Blaabjerg F et al (2013) Analysis of the passive damping losses in LCL-filter-based grid converters. IEEE Trans Power Electron 28(6):2642–2646

[4] Tang Y, Loh PC, Wang P et al (2012) Generalized design of high performance shunt active power filter with output LCL filter. IEEE Trans Ind Electron 59(3):1443–1452

[5] He J, Li Y (2012) Generalized closed-loop control schemes with embedded virtual impedances for voltage source converters with LC or LCL filters. IEEE Trans Power Electron 27(4):1850–1861

[6] Zou Z, Wang Z, Cheng M et al (2014) Modeling, analysis, and design of multifunction grid-interfaced inverters with output LCL filter. IEEE Trans Power Electron 29(7):3830–3839

[7] Xiao H, Qu X, Xie S (2012) Synthesis of active damping for grid-connected inverters with an LCL filter. In: Proceedings of 2012 IEEE energy conversion congress and exposition (ECCE) meeting, Edinburgh, Scotland, 28–31 Aug 2012, 7 pp

[8] Hanif M, Khadkikar V, Xiao W et al (2014) Two degrees of freedom active damping technique for filter-based grid connected PV systems. IEEE Trans Ind Electron 61(6):2795–2803

[9] Xu J, Xie S, Tang T (2014) Active damping-based control for grid-connected filtered inverter with injected grid current feedback only. IEEE Trans Ind Electron 61(9):4746–4758

[10] Tang Y, Loh PC, Wang P et al (2012) Exploring inherent damping characteristic of LCL-filters for three-phase grid-connected voltage source inverters. IEEE Trans Power Electron 27(3):1433–1443

[11] Dannehl J, Fuchs FW, Hansen S et al (2010) Investigation of active damping approaches for PI-based current control of grid-connected pulse width modulation converters with LCL filters. IEEE Trans Ind Appl 46(4):1509–1517

[12] Parker SG, McGrath B, Holmes D (2014) Regions of active damping control for LCL filters. IEEE Trans Ind Appl 50(1):424–432

[13] Ghoshal A, John V (2015) Active damping of LCL filter at low switching to resonance frequency ratio. IET Trans Power Electron 8(4):574–582

[14] Lyu Y, Li H, Cui Y (2015) Stability analysis of digitally controlled LCL type grid-connected inverter considering the delay effect. IET Trans Power Electron 8(9):1600–1651

[15] Pan D, Ruan X, Bao C et al (2014) Capacitor-current-feedback active damping with reduced computation delay for improving robustness of LCL-type grid-connected inverter. IEEE Trans Power Electron 29(7):3414–3427

[16] Yin J, Duan S, Liu B (2013) Stability analysis of grid-connected inverter with LCL filter adopting a digital single-loop controller with inherent damping characteristic. IEEE Trans Ind Inform 9(2):1104–1112

[17] Wang J, Yan JD, Jiang L et al (2016) Delay-dependent stability of single-loop controlled grid-connected inverters with LCL filters. IEEE Trans Power Electron 31(1):743–757

[18] Li W, Ruan X, Pan D et al (2013) Full-feedforward schemes of grid voltages for a three-phase type grid-connected inverter. IEEE Trans Ind Electron 60(6):2237–2250

[19] Wang X, Ruan X, Liu S et al (2010) Full feed-forward of grid voltage for grid-connected inverter with LCL filter to suppress current distortion due to grid voltage harmonics. IEEE Trans Power Electron 25(12):3119–3127

[20] Tang Y, Yao W, Loh PC et al (2016) Design of LCL filters with LCL resonance frequencies beyond the Nyquist frequency for grid-connected converters. IEEE J Emerg Sel Top Power Electron 4(1):3–14

[21] Davison DM et al (2001) Control system design (Goodwin, G.C. et al; 2001) book review. IEEE Control Syst 27(1):77–79

[22] Mukherjee N, De D (2013) Analysis and improvement of performance in LCL filter-based PWM rectifier/inverter application using hybrid damping approach. IET Trans Power Electron 6(2):309–325

[23] Agorreta JL, Borrega M, López J et al (2011) Modeling and control of paralleled grid-connected inverters with LCL filter coupled due to grid impedance in PV plants. IEEE Trans Power Electron 26(3):770–785

[24] Bao C, Ruan X, Wang X et al (2014) Step-by-step controller design for LCL-type grid-connected inverter with capacitor–current-feedback active-damping. IEEE Trans Power Electron 29(3):1239–1253

[25] Li B, Yao W, Hang L et al (2012) Robust proportional resonant regulator for grid-connected voltage source inverter (VSI) using direct pole placement design method. IET Power Electron 5(8):1367–1373

Wei XIA received the B. Eng. and M. Eng. degrees in Electrical Engineering from Wuhan University of Technology, Wuhan, China, in 2004 and 2007, respectively. He was with Shanghai Electrical Apparatus Research Institute, China, for 6 years, engaged in the R&D of PV system. Since 2013, as a Ph.D candidate, he has been with the School of Electronics and Information Engineering, Tongji University, Shanghai, China. His research interests include the control of power electronics and renewable energy generation system.

Jinsong KANG received the B.Eng. and M.Eng. degrees from Shanghai Railway University, Shanghai, China, in 1994 and 2000, respectively, and the Ph.D from Tongji University, Shanghai, China in 2003, all in Electrical Engineering. He is currently a Professor at Tongji University with research interests in power electronics-based inverter systems for grid connection of renewable power generation or drive system of electric vehicles.